Enhanced Automatic Lung Segmentation Using Graph Cut for Interstitial Lung Disease

Joel Than Chia Ming, *MIEEE*, Norliza Mohd Noor, *SMIEEE*, Omar Mohd Rijal, *MIEEE*, Rosminah M. Kassim, Ashari Yunus

***Abstract*— Radiologists are known to suffer from fatigue and drop in diagnostic accuracy due to large number of slices to read and long working hours. A computer aided diagnosis (CAD) system could help lighten the workload. Segmentation is the first step in a CAD system. This study aims to propose an accurate automatic segmentation. This study deals with High Resolution Computed Tomography (HRCT) scans of the thorax for 15 healthy patients and 81 diseased lungs segregated to five levels based on anatomic landmarks by a senior radiologist. The method used in this study combines thresholding and normalized graph cut which is a combination of region and contour based methods. The way the graph cut is implemented with a rule of exclusion can offer some knowledge for greater accuracy of segmentation. The segmentation was compared to manual tracing done by a trained person who is familiar with lung images. The segmentation yielded 98.32% and 98.07% similarity for right lung (RL) and left lung (LL). The segmentation error of Relative Volume Difference (RVD) for both RL and LL are also low at 0.89% and -0.13% respectively. The Overlap Volume Errors (OVE) are low at 3.17% and 3.74% for RL and LL. Thus the automatic segmentation proposed was able to segment accurately across right and left lung and was able to segment severe diseased lungs.**

I. Introduction

Radiologists today deal with a heavy workload that leads to fatigue, causing a drop in diagnostic accuracy[1]. There is growing interest in developing a Computer Aided Diagnosis (CAD) system to help radiologists and clinicians to reduce workload and increase diagnostic accuracy. CAD systems have shown to help especially radiologists with little experience and also in breast cancer diagnosis[2], [3]. The first important in building such a system is developing a segmentation component. A segmentation algorithm might be specific to a disease or general in application.

*Research supported by the Research University Grant: GUP QK130000.2540.06H35, Universiti Teknologi Malaysia and Ministry of Higher Education.

Joel Chia Ming Than, is a Master student (by research) at UTM Razak School of Engineering and Advanced Technology, Universiti Teknologi Malaysia, Malaysia (corresponding author tel.: +60146887078.; fax: +603-21805380; email: tcmjoel2@live.utm.my).

N. M. Noor is with the Department of Engineering, UTM Razak School of Engineering and Advanced Technology, Universiti Teknologi Malaysia, Malaysia (e-mail: norliza@utm.my).

O. M. Rijal is with the Institute of Mathematical Sciences, Faculty of Science, University of Malaya, Kuala Lumpur, Malaysia (e-mail: omarrija@um.edu.my).

R. M. Kassim, is with the Department of Diagnostic Imaging, Kuala Lumpur Hospital (e-mail: rosminahmk@yahoo.com).

A. Yunus is with the Institute of Respiratory Medicine, Malaysia (e-mail: ashdr64@yahoo.com.au).

Interstitial Lung Disease (ILD) is a wide category of chronic diseases that share common traits specifically physiologic and radiologic traits [4], [5]. These radiologic traits are important for detection and are seen through High Resolution Computed Tomography (HRCT). It is proven that using a limited number of HRCT slices based on anatomic landmarks is sufficient for ILD diagnosis[6]. These limited thin sections are levels and can be done in three or five levels[7].Therefore this study will be using the five level system. ILD can be caused by many factors such as exposure to hazardous materials, genetic factors and Rheumatoid Arthritis [8], [9].

There are many categories of segmentation methods but there are two main categories that most methods adhere to. The first is region based methods which utilize information of the pixels, regions and intensity. These methods have a weakness of having inaccurate borders. Region growing is a popular example where a seed point selected and then the connectivity of neighboring pixels are evaluated to be of the same characteristic [10]. Second category is contour based which utilizes edge detection and a linking process to link all the edges.

Most methods include threshold manipulation as one of the main techniques. Hu et. al. did a study that showed the first automated segmentation which drew much attention [11]. Other methods include but not limited to watershed method[12], [13] active contours or snakes [14],graph cut methods[15].

However segmentation faces a problem when there are diseased lungs. This requires specialized algorithms and methods. Thus the aim of this study is to produce and evaluate an accurate automatic segmentation method that is enhanced to deal with inconsistent segmentation due to scaring and diseased problem. This will be done using two main concepts of thresholding and graph cut which combines both region and contour based methods.

II. Data Collection

A. HRCT Slices

HRCT Thorax images were obtained from the Department of Diagnostic imaging of Kuala Lumpur retrospectively for this study with ethical clearance received for research purposes. In total there were 96 patients consisting 15 healthy (normal cases), 28 ILD patients (ILD cases) and 53 non-ILD lung related diseases (non-ILD cases). There were 48 male and 48 female patients. Images were recorded using Siemens SomatomPlus4 CT scanner. Each slice was attained at 10 – 30 mm intervals of patients in supine position will

978-1-4799-4084-4/14/$31.00 ©2014 IEEE

full suspended inspiration. Most images are saved in size 512 x 512, DICOM format. All images with size 1024x1024, they are converted to size 512 x 512, DICOM format.

B. Five Level Determination

A senior radiologist is appointed to view the HRCT slices using SyngoFastView version VX57G27 and determine the five levels (L1 – L5) of each patient based on anatomic landmarks specific as follows; L1: Aortic arch, L2: Trachea carina, L3: Pulmonary hilar , L4: Pulmonary venous confluence and L5: 1- 2 cm above the dome of right hemi-diaphragm

III. Methodology

This study is the further progress and improvement based on two previous studies [7], [16] with the enhancement of graph cut. Although these methods are known methods, the ways and steps for it to be used and parameters involved can be of value and unique. The steps involved are applied on all 96 patients and is fully automatic.

All images were first processed with the initial automatic lung segmentation based on thresholding and morphology. Next, severe cases where the initial segmentation was erroneous was enhanced with normalized graph cut.

A. Initial Automatic Lung Segmentation

HRCT lung images were processed accordingly using thresholding first which utilizes morphological filtering and global thresholding method to extract out regions of interest or in this study's context it is the right lung and left lung. The overall segmentation steps are shown in Figure 1. Firstly the body region is separated from surrounding with a global gray level threshold which is Otsu Thresholding [17]. This utilizes the contrasts of each pixel. Generally lung tissue contains air thus have different contrasts than that of the body tissue. The effect of this is shown in Fig 1(b).

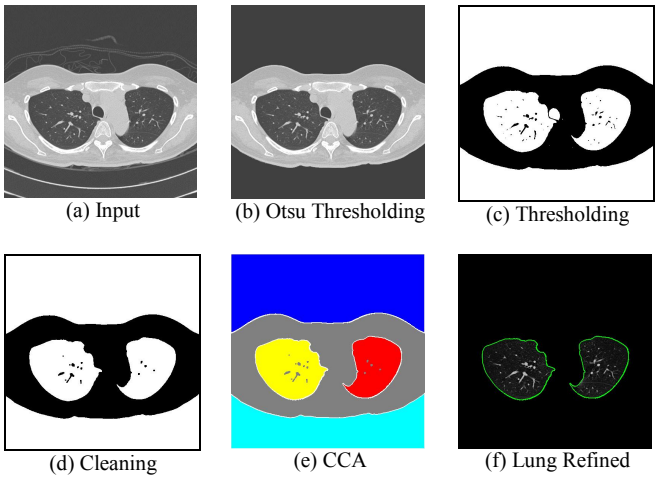

(a) Input (b) Otsu Thresholding (c) Thresholding

(d) Cleaning (e) CCA (f) Lung Refined

Figure 1. Initial Lung Segmentation Steps

An empirical threshold of -324HU is used an applied to obtained separation of lung and body as seen in Fig 1(c). Next the images are morphologically filtered using morphological closing yielding the output in Figure 1(d). Then in order for lungs to be located and are identified as the left and the right lung, Connected Component Analysis (CCA). CCA will separate the regions based on connectivity and label them with colors as seen in Figure 1(e). If two lungs are not present, radon transform, pixel width accumulation and processing are used to obtain two lung regions [16]. The lungs are refined and the borders are obtained as green borders in Fig 1(f). All morphological operation uses a 'square' structure element of '3x3' pixel size.

B. Normalized Graph Cut Enhancement

The normalized graph cut method used follows the renowned graph cut method for segmentation [18], [19]. However, the steps involved in post processing and obtaining the lung region in this study are unique and can offer new knowledge in image processing. A graph cut is defined as the dissimilarity between two regions of points A and B. The union of A and B *will yield* V. This dissimilarity can be calculated as the removal of the connecting edges of A and B termed as weight, w as shown in equation 1.

$$cut(A,B) = \sum_{u \in A, v \in B} w(u,v) \tag{1}$$

where u and v are points in region A and B respectively.

The normalized graph cut is the ratio of graph cut to connection of points in region A to all points in V, given by $assoc(A,V)$, summed together with ratio of graph cut to connection of points in region B to all points in V, given by $assoc(B,V)$ as shown in equation 2.

$$Ncut(A,B) = \frac{cut(A,B)}{assoc(A,V)} + \frac{cut(A,B)}{assoc(B,V)} \tag{2}$$

The implementation of this normalized graph cut may be unique and the extraction of the regions segmented can be intuitive and offer some insight to better segmentation. For this study, severe diseased images were enhanced with normalized graph cut after the initial segmentation. For all enhanced cases, the normalized graph cut was set to cut 45 segments in each image. This number is empirically chosen to represent sufficient segments to split up different regions of the lung.

The enhancement proposed here is because of the errors from the initial segmentation. For example for an input of Fig2 (a) the error from initial segmentation, where there is under-segmentation for the right lung as seen in Fig 2(b). To implement graph cut it involves steps preprocessing and post processing to ensure good segmentation as listed below;

1. Removal of opposing lung region seen in Fig 2(c).
2. Normalized Graph Cut executed with 45 segments seen in Fig 2(d).
3. Segments of the lung are automatically just as Fig 2(e) selected based on three criteria of exclusion below;

a. Segments are not connected to region of opposing lung.

b. Segments are not connected to the body boundary.

c. Segments do not contain more than 50% of non-lung region defined by a threshold.

4. Any lung pixels are added in from the initial segmentation based on thresholding and morphology.

5. The lung is region with refined with erosion and dilation to remove non lung components from the segments. The refined lung is shown in Fig 2(f)

The opposing lung is removed in the first step to enable easier segmentation where only one lung will be evaluated. This saves computation time and steps involved. The 45 segments yielded from the execution normalize graph cut are high in number to ensure the lungs regions are within the segments. The segments are chosen based on the three criteria that eliminate out non lung segments. The segments selected are refined with erosion and dilation to ensure smooth lung borders and eliminate connecting non lung objects.

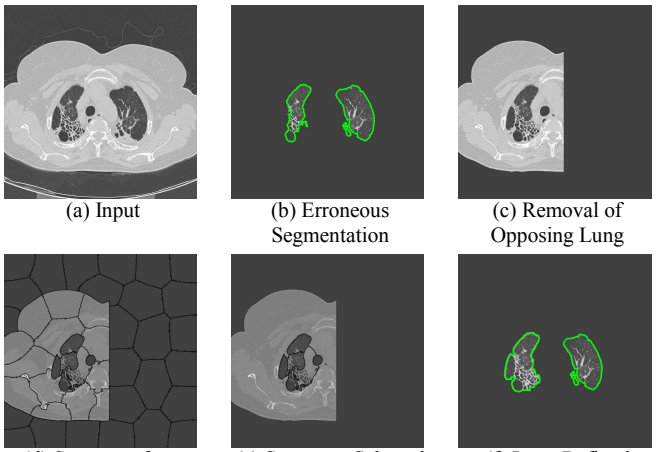

(a) Input (b) Erroneous Segmentation (c) Removal of Opposing Lung

(d) Segments from Normalized Graph Cut (e) Segments Selected (f) Lung Refined

Figure 2. Enhanced Segmentation Steps with Graph Cut

IV. Performance Evaluation

The automatic segmentation results were compared with the manual tracing done by a person sufficiently trained in lung images to determine the lung boundaries. The comparison was done using several performance evaluation measures. The first measure is Dice Similarity Coefficient (DSC) shows the degree of area that is overlapping between the segmented image (A) and manual tracing (B) shown in equation 3.

$$DSC = \frac{2(A \cap B)}{A \cup B} \times 100\% \quad (3)$$

The second performance measure is Relative Volume Difference (RVD), which is a measure of percentage of the difference segmented (A) and the manual tracing volume (B) divided by the reference volume given below in equation 4.

$$RVD = \frac{A - B}{B} \times 100\% \quad (4)$$

$$OVE = 1 - \frac{A \cap B}{A \cup B} \times 100\% \quad (5)$$

The third measure Volume Overlap Error (VOE) is a volume based error measurement which yields a value in percentage. VOE is the ratio of the areas that are not intersecting to the union between the segmented region (A) and the manual tracing region (lB) which in this study is the manual tracing. VOE is based on the Jaccard's coefficient and is shown in equation 5[20].

The Bland-Altman Plot is also used to show the similarity between the segmented and manual tracing. The plot is made out of 2 axis, the horizontal representing the average between the segmented and manual tracing and the vertical representing the difference between the segmented and manual tracing [21].

V. Results

The segmentation method was applied on all five levels and yielded high accuracy. In this section, the accuracy and performance of the segmentation is presented. Firstly the performance can be represented visually. This is represented in the overlay of the segmentation boundary represented by green boundary and manual tracing boundary represented by red boundary.

The high similarity between the two boundaries is represented by the almost complete overlap of the manual tracing boundary by the segmentation boundary shown in Figure 3. The red boundary is almost in-distinguishable from the green boundary. For diseased lungs, the enhancement of graph cut brought the boundaries of segmentation (green) closer to the boundaries of manual tracing (red) for both right lung (RL) and left lung (LL) as shown in Figure 4.

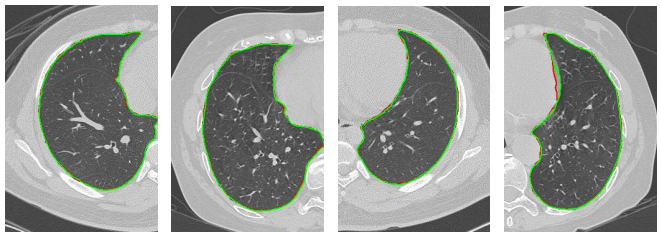

Figure 3. Example of Good Segmentation

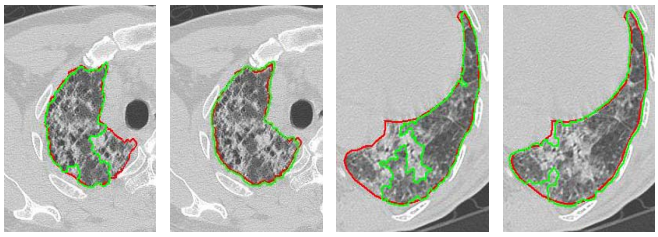

(i) (ii) (iii) (iv)

Figure 4. Example of Before and After Enhancement of Graph Cut: (i) Before (RL), (ii) After (RL), (iii) Before (LL), (iv) After (LL)

The performance of the segmentation is also presented in numerical form in Table 1 and Table 2. The Dice Similarity Coefficient (DSC) values for the right lung and left lung are consistently high for all five levels. The overall mean for right and left lung are above 98% which are 98.32% and 98.07% respectively signifying high accuracy.

TABLE I. RIGHT LUNG PERFORMANCE

Level	DSC		RVD		OVE	
	Mean	*±SD*	*Mean*	*±SD*	*Mean*	*±SD*
L1	97.92	6.15	3.33	26.48	3.59	8.22
L2	98.39	1.59	0.27	3.32	3.13	2.95
L3	98.32	1.43	0.55	3.46	3.26	2.68
L4	98.25	1.45	0.04	3.18	3.41	2.68
L5	98.73	1.33	0.36	3.01	2.47	2.46
Mean	98.32	2.99	0.89	11.99	3.17	4.34

TABLE II. LEFT LUNG PERFORMANCE

Level	DSC		RVD		OVE	
	Mean	*±SD*	*Mean*	*±SD*	*Mean*	*±SD*
L1	98.70	1.08	0.27	2.21	2.54	2.02
L2	98.42	1.06	-0.51	2.35	3.10	2.00
L3	98.16	1.36	-0.04	2.47	3.58	2.52
L4	97.43	2.08	0.10	5.08	4.93	3.79
L5	97.66	2.23	-0.43	3.64	4.49	4.00
Mean	98.07	1.70	-0.13	3.34	3.74	3.11

The Relative Volume Difference (RVD) for both right lung and left lung are also low at 0.89% and -0.13% respectively. The negative values indicate that the segmentation is smaller than the manual tracing and vice versa. The Overlap Volume Error (OVE) for both right and left lung are low at 3.17% and 3.74% respectively.

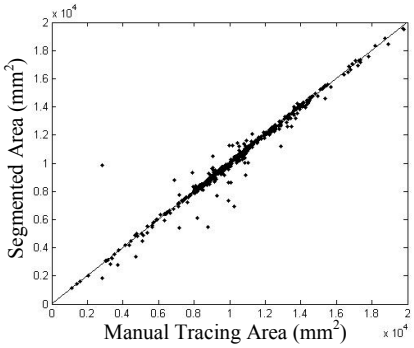

Figure 5. Scatter Plot of Lung Area (Right Lung)

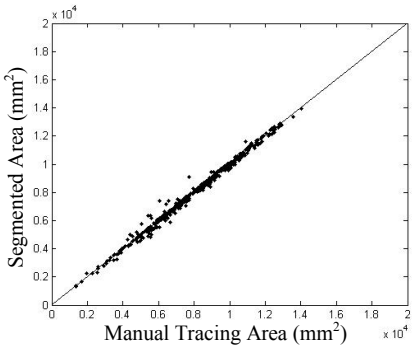

Figure 6. Scatter Plot of Lung Area (Left Lung)

The scatter plots for RL and LL shown in Figures 6 and 7 exhibit the high consistency of the segmentation method across increasing area of the lung. The points are close to the trendline signifying the similarity to the manual tracing. Bland Altman plots in Figure 7 and 8 represent the agreement between manual tracing and segmentation. It can be seen most of the points are within the ranges of 2SD signified by the dotted lines. This shows that most of the segmentations are in agreement with the manual tracing.

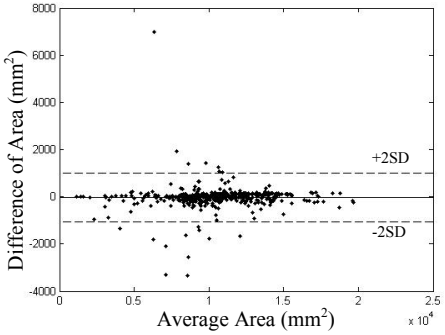

Figure 7. Bland-Altman Plot of Lung Area (Right Lung)

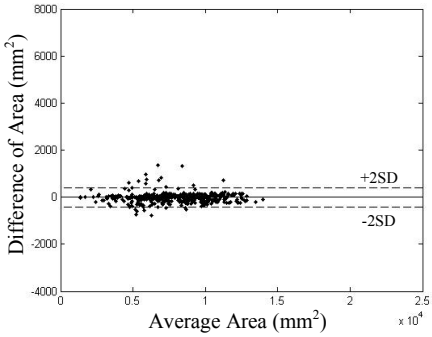

Figure 8. Bland-Altman Plot of Lung Area (Left Lung)

VI. DISCUSSION & CONCLUSION

The study has proposed a segmentation method that uses thresholding and normalized graph cut. The implementation of the graph cut can be intuitive and offer steps for further application. The segmentation yielded high accuracy and was

able to deal with diseased lungs pushing the borders of segmentation closer to that of the manual tracing.

From the results in the previous section it is exhibited that segmentation proposed would be able to yield high accuracy. This is seen visually in the form of overlays as well as numerically in the form of performance measures. There is similarity where the majority of levels for both right and left lung yield more than 98% of similarity. The overall similarity is also above 98% for both lungs signifying accurate segmentation. This is also supported the low relative volume difference and overlap volume error.

The segmentation proposed also was able to perform across all five levels of the lung for both right and left lung. This shows the ability of the segmentation to deal with variability not only whether the sample is diseased or healthy but also at different slices of the lung.

A limitation of this segmentation so far is applied on 2D images for this study and will be applied and modified for 3D images in the future. Another limitation is that only one observer is tasked to do manual tracing. For future works, inter-observer and intra-observer variability could be investigated to further to validate the accuracy of segmentation.

As a conclusion, the automatic segmentation proposed was able to show high performance and similarity to the manual tracing of 98.32% and 98.07% across all five levels of diseased and normal lungs for both right and left lung thus signifying an accurate segmentation method.

REFERENCES

[1] E. A. Krupinski, K. S. Berbaum, R. T. Caldwell, K. M. Schartz, and J. Kim, "Long radiology workdays reduce detection and accommodation accuracy," *J. Am. Coll. Radiol.*, vol. 7, no. 9, pp. 698–704, 2010.

[2] T. Kobayashi, X.-W. Xu, H. MacMahon, C. E. Metz, and K. Doi, "Effect of a computer-aided diagnosis scheme on radiologists' performance in detection of lung nodules on radiographs.," *Radiology*, vol. 199, no. 3, pp. 843–848, 1996.

[3] F. Beyer, L. Zierott, E. M. Fallenberg, K. U. Juergens, J. Stoeckel, W. Heindel, and D. Wormanns, "Comparison of sensitivity and reading time for the use of computer-aided detection (CAD) of pulmonary nodules at MDCT as concurrent or second reader.," *Eur. Radiol.*, vol. 17, no. 11, pp. 2941–7, Nov. 2007.

[4] T. Peroš-Golubičić and O. Sharma, *Clinical atlas of interstitial lung disease*. Springer, 2006.

[5] R. G. Crystal, J. E. Gadek, V. J. Ferrans, J. D. Fulmer, B. R. Line, and G. W. Hunninghake, "Interstitial lung disease: Current concepts of pathogenesis, staging and therapy," *Am. J. Med.*, vol. 70, no. 3, pp. 542–568, Mar. 1981.

[6] E. A. Kazerooni, F. J. Martinez, A. Flint, D. A. Jamadar, B. H. Gross, D. L. Spizarny, P. N. Cascade, R. I. Whyte, J. P. Lynch, G. Toews, and J. P. Lynch 3rd, "Thin-section CT obtained at 10-mm increments versus limited three-level thin-section CT for idiopathic pulmonary fibrosis: correlation with pathologic scoring.," *AJR. Am. J. Roentgenol.*, vol. 169, no. 4, pp. 977–983, 1997.

[7] N. M. Noor, O. M. Rijal, J. Than, C. Ming, F. A. Roseli, J. T. C. Ming, H. Ebrahimian, R. M. Kassim, and A. Yunus, "Segmentation of the Lung Anatomy for High Resolution Computed Tomography (HRCT) Thorax Images," in *Advances in Visual Informatics*, no. Ild, Springer, 2013, pp. 165–175.

[8] P. Sharman and R. Wood-Baker, "Interstitial lung disease due to fumes from heat-cutting polymer rope.," *Occup. Med. (Lond).*, vol. 63, no. 6, pp. 451–3, Sep. 2013.

[9] D. N. O'Dwyer, M. E. Armstrong, G. Cooke, J. D. Dodd, D. J. Veale, and S. C. Donnelly, "Rheumatoid Arthritis (RA) associated interstitial lung disease (ILD).," *Eur. J. Intern. Med.*, vol. 24, no. 7, pp. 597–603, Oct. 2013.

[10] J. Dehmeshki, H. Amin, M. Valdivieso, and X. Ye, "Segmentation of pulmonary nodules in thoracic CT scans: a region growing approach," *Med. Imaging, IEEE Trans.*, vol. 27, no. 4, pp. 467–480, 2008.

[11] S. Hu, E. a Hoffman, and J. M. Reinhardt, "Automatic lung segmentation for accurate quantitation of volumetric X-ray CT images.," *IEEE Trans. Med. Imaging*, vol. 20, no. 6, pp. 490–8, Jun. 2001.

[12] J. J.-M. Kuhnigk, H. Hahn, M. Hindennach, V. Dicken, S. Krass, and H.-O. Peitgen, "Lung lobe segmentation by anatomy-guided 3D watershed transform," in *Medical Imaging 2003*, 2003, vol. 4, no. 01, pp. 1482–1490.

[13] R. Shojaii, J. Alirezaie, and P. Babyn, "Automatic lung segmentation in CT images using watershed transform," in *Image Processing, 2005. ICIP 2005. IEEE International Conference on*, 2005, vol. 2, pp. II–1270–3.

[14] A. Osareh and B. Shadgar, "A segmentation method of lung cavities using region aided geometric snakes," *J. Med. Syst.*, vol. 34, no. 4, pp. 419–433, 2010.

[15] L. Massoptier, A. Misra, and A. Sowmya, "Automatic lung segmentation in HRCT images with diffuse parenchymal lung disease using graph-cut," in *Image and Vision Computing New Zealand, 2009. IVCNZ'09. 24th International Conference*, 2009, pp. 266–270.

[16] J. Chia, M. Than, N. M. Noor, O. M. Rijal, A. Yunus, and R. Kassim, "Lung Segmentation for HRCT Thorax Images using Radon Transform and Accumulating Pixel Width," 2014, pp. 161–165.

[17] N. Otsu, "A threshold selection method from gray-level histograms," *Automatica*, vol. 11, no. 285–296, pp. 23–27, 1975.

[18] J. Shi and J. Malik, "Normalized cuts and image segmentation," *Pattern Anal. Mach. Intell. IEEE Trans.*, vol. 22, no. 8, pp. 888–905, 2000.

[19] Y. Boykov and M.-P. Jolly, "Interactive organ segmentation using graph cuts," in *Medical Image Computing and Computer-Assisted Intervention--MICCAI 2000*, 2000, pp. 276–286.

[20] P. Jaccard, "Nouvelles recherches sur la distribution florale.," *Bull. Soc. Vaudoise Sci. Nat.*, vol. 44, pp. 223–270, 1908.

[21] J. Martin Bland and D. Altman, "Statistical methods for assessing agreement between two methods of clinical measurement," *Lancet*, vol. 327, no. 8476, pp. 307–310, 1986.